Journal of Power Sources 194 (2009) 1053–1060

Contents lists available at ScienceDirect

Journal of Power Sources

journal homepage: www.elsevier.com/locate/jpowsour

Effect of combinations of additives on the performance of lithium ion batteries

Stuart Santee[a,b], Ang Xiao[a], Li Yang[a], Joe Gnanaraj[b], Brett L. Lucht[a,*]

[a] Department of Chemistry, University of Rhode Island, 51 Lower College Rd., Kingston, RI 02881, United States
[b] Lithion Inc., 82 Mechanic St., Pawcatuck, CT 06379, United States

ARTICLE INFO

Article history:
Received 4 May 2009
Received in revised form 4 June 2009
Accepted 5 June 2009
Available online 12 June 2009

Keywords:
Lithium-ion batteries
Electrolytes
Thermal stability
Performance degradation

ABSTRACT

Commercial lithium-ion batteries have excellent performance at room temperature for a few years. However, the calendar life and thermal stability (>50 °C) need to be improved for many applications, including electric vehicles. We have conducted an investigation of the effect of thermal stabilizing additives, including dimethyl acetamide, vinylene carbonate, and lithium bis(oxalato) borate, on the performance of lithium ion batteries stored at 70 °C for one month. The reactions of the lithium hexafluorophosphate/carbonate electrolyte, with and without electrolyte additives, with the surface of the electrodes after initial formation cycling have been analyzed via a combination of IR-ATR and XPS.

1. Introduction

Lithium-ion batteries (LIB) have been widely used for portable consumer electronic applications. However, they have several problems including limited operating temperature and loss of power and capacity upon storage or prolonged use. While there are several factors that limit the thermal stability of LIB, the reactions of the electrolyte with the surface of the electrode materials is frequently reported to be the most important [1]. The most extensively used $LiPF_6$ electrolytes have poor thermal stability. Therefore, inhibition of the detrimental thermal reactions of the electrolyte with the surface of the electrode materials (both cathode and anode) will lead to enhanced thermal stability of high energy LIB.

Earlier studies have investigated the mechanisms of the thermal decomposition of $LiPF_6$ based electrolytes. It has been found that during the thermal decomposition of $LiPF_6$ based electrolytes, PF_5 reacts rapidly with trace protic impurities in the electrolyte, such as water, to form OPF_3, which then initiates an auto-catalytic decomposition of the electrolyte [2,3]. This paper is a study of a number of thermal stabilizing additives and combinations of these additives in LIB.

Electrolyte solvents capable of good performance in LIBs are those which possess an ability to stabilize the graphite anode by forming a protective solid electrolyte interphase (SEI) which inhibits further reactions of the electrolyte while permitting Li^+ charge transfer between the anode and the electrolyte [4]. Enhancing the stability of the anode SEI has typically been conducted via the addition of sacrificial additives, which are more easily reduced than ethylene carbonate (EC) and form a thermally stable anode SEI. Two of the most interesting additives are vinylene carbonate (VC) [5,6] and lithium bis(oxalato)borate (LiBOB) [7–9]. Alternatively, one can stabilize the bulk electrolyte. Lewis bases such as dimethyl acetamide (DMAc) stabilize $LiPF_6$ electrolytes by complexing the Lewis acidic PF_5 generated during the thermal dissociation of $LiPF_6$. The DMAc-PF_5 complex inhibits the reaction of PF_5 with the carbonate solvent and subsequent auto-catalytic decomposition reaction [2,3,10]. The inhibition of the thermal decomposition of $LiPF_6$ electrolytes via addition of DMAc subsequently protects the anode SEI by preventing the formation of reactive species that degrade the SEI.

The goal of this work is to identify and develop electrolyte additives which will lead to LIBs with a wider operating temperature range. In particular, this is a study of the effect of a small amount (1–5%) of DMAc, VC, and/or LiBOB to the $LiPF_6$/carbonate electrolytes frequently used in commercial and specialty LIB. The examination of the thermal stability was conducted with a 1.0 M $LiPF_6$ solution in EC/DMC/DEC (1/1/1) as a standard electrolyte with and without additives. The cells were stored 70 °C for a 30 day period followed by electrochemical analysis.

2. Experimental

The active material for the anode is Mesophase Carbon Microbeads (MCMB 6–28). The active material for the cathode is $LiNi_{0.8}Co_{0.2}O_2$. The ratio of active material was 1.3:1 (MCMB/$LiNi_{0.8}Co_{0.2}O_2$). Polyvinylidene fluoride (PVDF), is used for

* Corresponding author. Tel.: +1 401 874 5071; fax: +1 401 874 5072.
E-mail address: blucht@chm.uri.edu (B.L. Lucht).

0378-7753/$ – see front matter © 2009 Elsevier B.V. All rights reserved.
doi:10.1016/j.jpowsour.2009.06.012

both anode and cathode. High surface area carbons are used in both the anode and cathode as conductive diluents. Slurries of powdered materials (~90% active material) are mixed in a humidity controlled environment. The slurries are then coated as thin films onto aluminum foil for the cathode and copper foil for the anode. The coatings are dried, passed through large rollers to compress the coatings (calendering), and blanked into the appropriate electrode size for cell construction. Cathodes are heat sealed in pouches of separator material made from thin film polyolefin.

Cycling for all cells was performed on Maccor Series 4000 Battery Testers. Thermal storage experiments were conducted with 12 Ah prismatic cells where a 1C discharge of the cell produces 12 A. All charges are at constant current until the cell voltage reaches 4.1 V. Once the cell has reached 4.1 V, the cell is charged at constant potential and the current is allowed to decrease until it falls below a certain value. Cells rest after charge for a specified time. All discharges are at constant current until the cell voltage reaches 3.0 V. Cells rest after discharge. If the chamber temperature is changed by 10 °C or more, the cells will rest for a minimum of 6 h at the new temperature before they continue cycling. Multiple cells (2–4) were prepared for each electrolyte. Cell to cell variation was less than 3%.

After formation (cells being charge-discharged at 0.05C for 1 cycle, 0.1C for 2 cycles and 0.2C for 2 cycles) and cell acceptance testing (CAT, cells being tested for capacity at 0 °C, 10 °C, 20 °C and 30 °C, 72 h stand test at fully charged state, pulse discharge at 20 °C and peak discharge at 4.1 V), the samples were maintained in a temperature chamber at 20 °C. The cells were charged at 2.4 A to a voltage of 4.1 V. Once the cell has reached 4.1 V, the cell is charged at constant potential and the current is allowed to decrease until it falls below 0.24 A. The cells are moved to a temperature chamber set to 70 °C. The cells remain in the temperature chamber for 30 days. After 30 days, the cells are moved to a temperature chamber set to 20 °C. The cells are allowed to soak for a minimum of 6 h, followed by discharge at 6 A to a voltage cut-off of 3.0 V.

Pouch cells (~100 mAh) with identical electrode materials and related electrolytes were fabricated. Initial formation cycling (cells being charge-discharged at 0.05C for 1 cycle, 0.1C for 2 cycles and 0.2C for 2 cycles) was conducted on the pouch cells followed by disassembly, rinsing with DMC, and surface analysis of the cycled electrodes [11]. The pouch cells were not stored at 70 °C. X-ray photoelectron spectroscopy (XPS) was conducted with a PHI 5500 system using Al Kα radiation under ultra high vacuum. Depth dependent elemental composition was collected by Ar^+ ion sputtering with etching rate of approximately 1 nm min^{-1} for SiO_2. Lithium was not monitored due to its low inherent sensitivity and small change of binding energy. The universal carbon contamination peak at 284.8 eV or graphite at 284.3 eV in the electrode was used to check the binding energy scale and charging effects. The spectra obtained were analyzed by Multipak 6.1A software. Line syntheses of elemental spectra were conducted using Gaussian–Lorentzian curve fit with Shirley background subtraction. FTIR-ATR analyses of the electrodes were carried out with a Thermo Nicolet IR300 infrared spectroscopy with attenuated total reflectance accessory. The spectroscopy was contained in a glove bag with nitrogen purging. 128 Scans were collected for each sample at three different locations.

The composition of the electrolyte used in all of the cells was 1.0 M $LiPF_6$ solution in EC/DMC/DEC (1/1/1, vol) (STD) with and without additives. The additive concentrations in the 12 Ah cells was 2% LiBOB, 0.5% DMAc, 3% VC, 2% LiBOB and 1% DMAc, 2% LiBOB and 1.5% VC, 1% DMAC and 1.5% VC, 2% LiBOB and 1% DMAc and 1.5% VC. The additive concentrations in the 100 mAh pouch cells was 2% LiBOB, 1% DMAc, 1.5% VC, 2% LiBOB and 1% DMAc, 2% LiBOB and 1.5% VC, 1% DMAC and 1.5% VC, 2% LiBOB and 1% DMAc and 1.5% VC.

3. Results and discussion

3.1. Battery cycling and storage

By performing the same CAT before and after 30 days of storage at 70 °C, the changes in cell performance are easily identified. There are three specific aspects of testing that best elucidate the changes in cell performance. The most basic is discharge energy. Cells will deliver less energy under the same conditions after high temperature storage. The 12 Ah cells cycle from 0 °C to 30 °C as part of standard testing. Therefore, the first two aspects of cell performance discussed will be discharge energy at 0 °C and at 30 °C before and after storage at 70 °C. The third aspect of performance discussed will be DC resistance at 20 °C. The data presented in Figs. 1–4 is the average of at least 2 cells. The variability of the different cells was less than 3%.

Fig. 1 shows discharge capacity (Ah) vs. cycle number of 12 Ah cells cycled at different temperatures of 20 °C, 0 °C, 10 °C, 20 °C and 30 °C before and after high temperature storage at 70 °C for 30 days

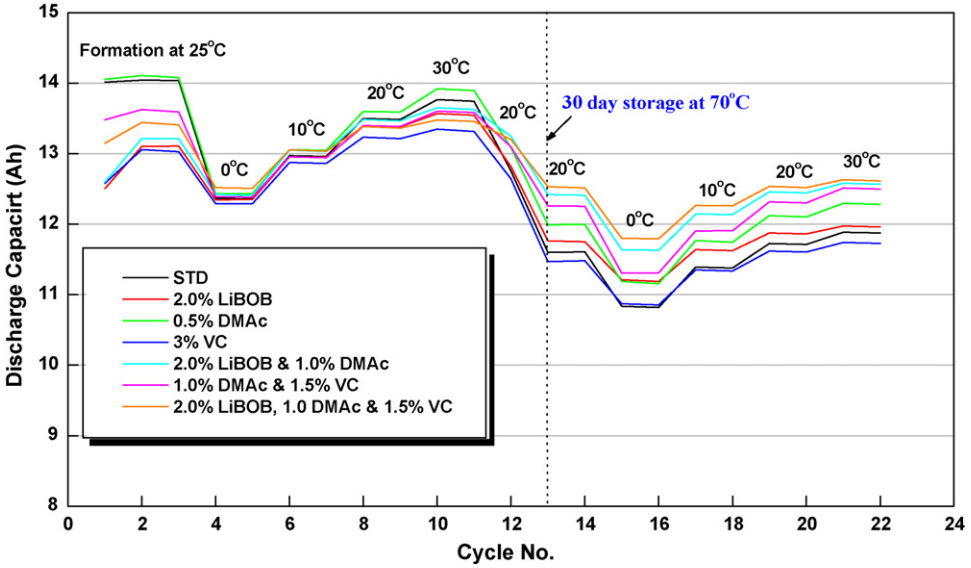

Fig. 1. Discharge capacities vs. cycle number plot for 12 Ah cells with and without electrolyte additives. The cells were cycled at 20 °C, 0 °C, 10 °C, 20 °C and 30 °C temperatures before and after high temperature storage at 70 °C for 30 days as indicated in the figure.

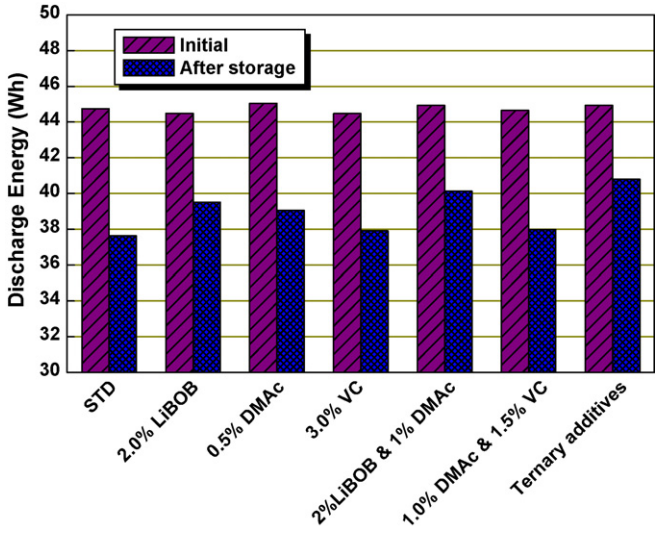

Fig. 2. Discharge energy (Wh) at 0 °C for all cells before and after 30 days storage at 70 °C.

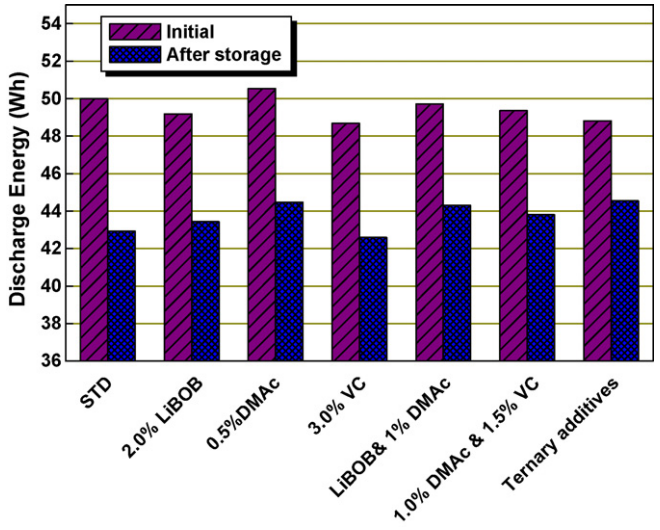

Fig. 3. Discharge energy (Wh) at 30 °C for all cells before and after each 30 days storage at 70 °C.

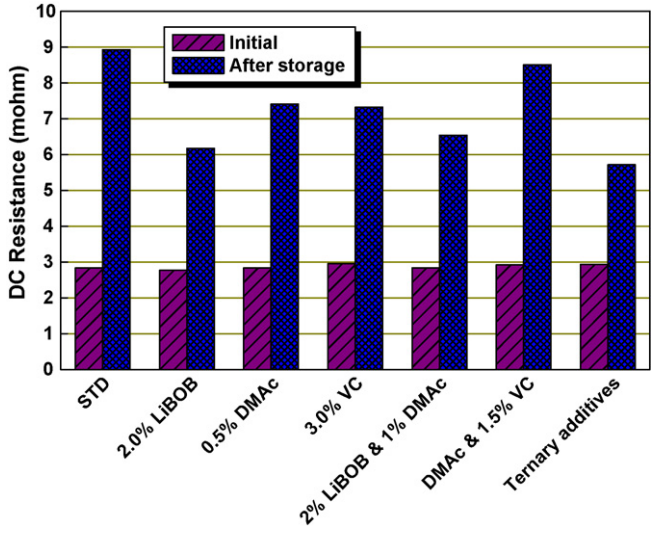

Fig. 4. DC resistance (mΩ) at 20 °C for all cells before and after each 30 days storage at 70 °C.

as indicated in the figure. The initial capacities for cells containing LiBOB or VC were lower than cells containing the standard electrolyte or the single additive DMAc consistent with the sacrificial nature of these additives [5–9]. However the capacity retention of cells containing any of the additives after high temperature storage was superior to that of the standard electrolyte. The cells containing combinations of additives (LiBOB and DMAc; DMAc and VC; and LiBOB, DMAc and VC) have better capacity retention than the standard electrolyte or any of the cells with a single additive.

Fig. 2 shows the discharge energy at 0 °C for all cells before and after 30 day storage at 70 °C. The mean discharge energy for all cells before storage was 44.7 Wh with a standard deviation of 0.28 Wh. This small variation shows the consistency of cell performance under these conditions regardless of the presence of additive. After the storage, the additive cells show variations with respect to the additives present. The standard cells all deliver less than 38 Wh retaining 84% of their discharge energy after the first storage.

The cells with 3% VC and 1.0% DMAc and 1.5% VC are all at or near 38 Wh. The cells with the highest retention all contained LiBOB as an additive. The best cells contained either LiBOB and DMAc and VC (91% retention) or LiBOB and DMAc (89% retention). The cells with DMAc and/or VC performed better than the standard cells but not as well as the cells containing LiBOB.

Fig. 3 shows the discharge energy at 30 °C for all cells before and after the 30 day storage at 70 °C. The mean discharge energy for all cells before storage was 49.6 Wh with a standard deviation of 0.80 Wh. There is greater variation in discharge energy at 30 °C than there is at 0 °C. Therefore, comparisons of discharge energy retention will better compare the performance of each additive or combination of additives.

The mean discharge energy results for testing at 30 °C are similar to the results for testing at 0 °C. All of the cells containing additives had better energy retention than the standard cells (85.8% retention). However, the cells containing VC only had only slightly better energy retention. The cells with the highest mean discharge energy retention at 30 °C after storage contained LiBOB and DMAc and VC and have 91.2% energy retention. The second and third highest were LiBOB and DMAc and DMAc and VC which had 89.1% and 88.7% retention respectively.

Fig. 4 shows the DC resistance at 20 °C for all cells before and after 30 day storage at 70 °C. The mean DC resistance for all cells before storage was 2.85 mΩ with a standard deviation of 0.08 mΩ. This small variation shows the consistency of cell performance under these conditions regardless of the presence of additive.

Comparisons of DC resistance changes are presented in Fig. 4. The cells with LiBOB and DMAc and VC have the smallest increase in DC resistance after storage (94.5%). This value is less than half of the value for the increase in DC resistance for the standard cells (215.6%). The LiBOB and DMAc and VC cells have a value less than half of the value for the cells with DMAc and VC (191.5%). The second smallest increase in DC resistance is associated with LiBOB as a single additive (123.2%). The third smallest increase in DC resistance is associated with LiBOB and DMAc (131.0%). This, along with the results in Figs. 1–3, is another example of the presence of LiBOB having a positive effect on performance retention. All cells containing additives performed better than the standard cells after storage at 70 °C for 30 days.

3.2. Analysis of surface films formed via reaction of the electrolyte with the electrode materials

Investigation of the composition of the SEI on both the cathode and the anode has been conducted by a combination of X-ray photoelectron spectroscopy (XPS) [11–14] and Infra-Red spectroscopy (FTIR) with attenuated total reflectance (ATR) [14,15]. The pouch cells had slightly different concentrations of additives that were

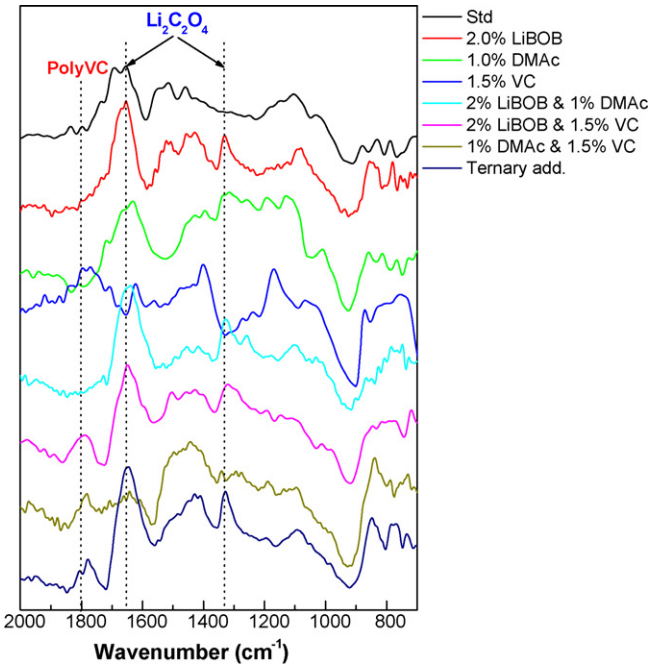

Fig. 5. FTIR-ATR of anodes with different additives.

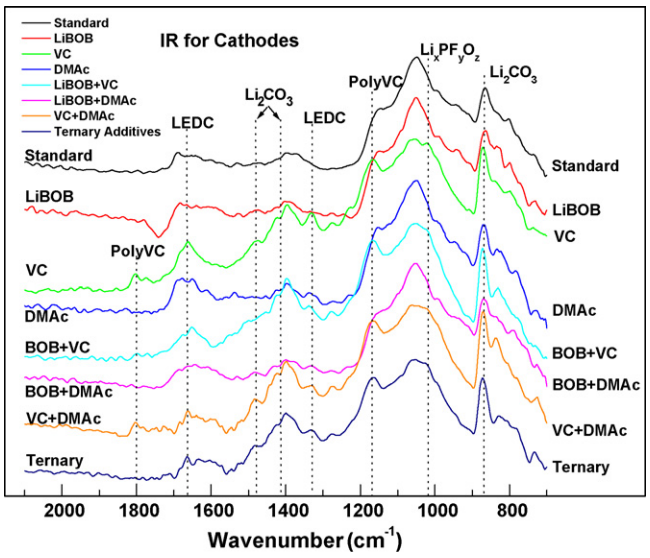

Fig. 6. FTIR-ATR of cathodes with different electrolyte additives.

incorporated into the 12 Ah cells described above. However, the electrode surface films should be very similar.

3.3. FTIR-ATR analysis of electrodes

Fig. 5 contains IR-ATR spectra of anodes extracted from the pouch cells described above, which have undergone standard formation cycling but no storage at 70 °C. The anode from a cell with standard ternary electrolyte mainly contains lithium alkyl carbonates $ROCO_2Li$ (characteristic of peaks at 2960 and 1635 cm^{-1}), carboxylate (1514 cm^{-1}), Li_2CO_3 (1426 cm^{-1} and 870 cm^{-1}) PVdF (1200 cm^{-1}), PEO (1100 cm^{-1}), and $Li_xPF_yO_z$ (900–1100 cm^{-1}) [14]. Recent investigations suggest that the cell design and handling influence the presence and quantity of Li_2CO_3 [16].

Addition of 2% LiBOB generates a novel and prominent peak at 1330 cm^{-1} compared to the standard sample, which is characteristic of either lithium oxalates or alkyl esters of oxalic acid as the products of rearranging reaction of LiBOB with semicarbonate-like compounds on SEI.

Samples containing DMAc have low concentrations of the electrolyte degradation products, especially lithium alkyl carbonates (1635 cm^{-1}) and $Li_xPF_yO_z$ (900–1100 cm^{-1}), suggesting reduced electrolyte decomposition. Presumably, DMAc inhibits the decomposition of electrolyte, primarily accounting for the change in composition of the SEI [10].

Samples containing VC are significantly different from the standard anode. Lower intensity peaks are observed for $ROCO_2Li$ (1635 cm^{-1}) and PEO (1100 cm^{-1}) in the SEI. However, several pronounced peaks represent the existence of polymeric species, such as polycarbonates (1790 cm^{-1}), and carboxylate (1514 cm^{-1}) [17,18], characteristic of a polymer layer on the surface of the graphite.

Anodes extracted from cells containing mixtures of additives have structural components consistent with a cooperative effect. Anodes from cells containing both LiBOB and DMAc have lower intensity of carboxylate (1514 cm^{-1}) absorptions. It appears that LiBOB and DMAc have a complementary effect to reduce the deposition of decomposition compounds on the SEI. In contrast to the sample containing VC, the sample with both VC and DMAc has a higher concentration of polycarbonates at 1790 cm^{-1}. A significant peak around 1790 cm^{-1} assigned to the poly(VC) is observed in samples containing LiBOB and VC, as well as in the sample with all three additives (LiBOB, VC, and DMAc). The new species is most likely due to reactions between the decomposition products of LiBOB and VC. The reductive process of oxalate moiety is around 1.70 V compared to VC around 1.50 V versus Li. The result of reaction between LiBOB and VC will modify the composition and morphology of SEI to generate novel SEI components.

Analysis of the surfaces of the cathodes extracted from the pouch cells described above by IR-ATR provides complementary results to those observed for the anode (Fig. 6). Signals from PVDF are observed at 1400, 1168, 1074 and 877 cm^{-1} in all samples. Peaks at 1635 and 843 cm^{-1}, which are characteristic of the RCO_3^- group, are assigned to alkylcarbonate species. The signal around 1790 cm^{-1} is characteristic of the carbonyl stretch of poly(VC). The peaks associated with poly(VC) are strongest with the VC and VC-DMAc samples, but are much weaker with the VC–LiBOB and VC–LiBOB–DMAc samples further suggesting that the combination of VC and LiBOB generate a anode SEI of unique structure. Peaks at 1426 and 870 cm^{-1} are attributed to Li_2CO_3. Lithium diethylene carbonate (LDEC) is also observed on the surface of the electrodes as evidenced by absorptions at 1310 and 1665 cm^{-1}.

3.4. XPS characterization of surface concentration of SEI on the anode

The surface composition of the anodes extracted from pouch cells that have undergone formation cycling only changed greatly upon the incorporation of the different additives, as evidenced by XPS (Figs. 7–12) and summarized in Table 1. All XPS spectra in

Table 1
Surface elemental concentration of SEI with different additives.

Sample	C1s	O1s	F1s	P2p	B1s
Fresh	62.1	3.3	34.6	–	–
Standard	30.5	16.4	51.4	1.7	–
LiBOB	33.5	22.6	39.9	0.2	3.8
DMAc	47.4	10.4	42.0	0.2	–
VC	43.6	12.9	43.5	0.0	–
LiBOB–DMAc	44.3	17.4	34.0	1.0	3.3
VC–DMAc	44.0	17.7	37.3	1.0	–
LiBOB–VC	47.6	21.2	28.5	1.0	1.6
LiBOB–VC–DMAc	49.2	20.1	29.7	0.4	0.6

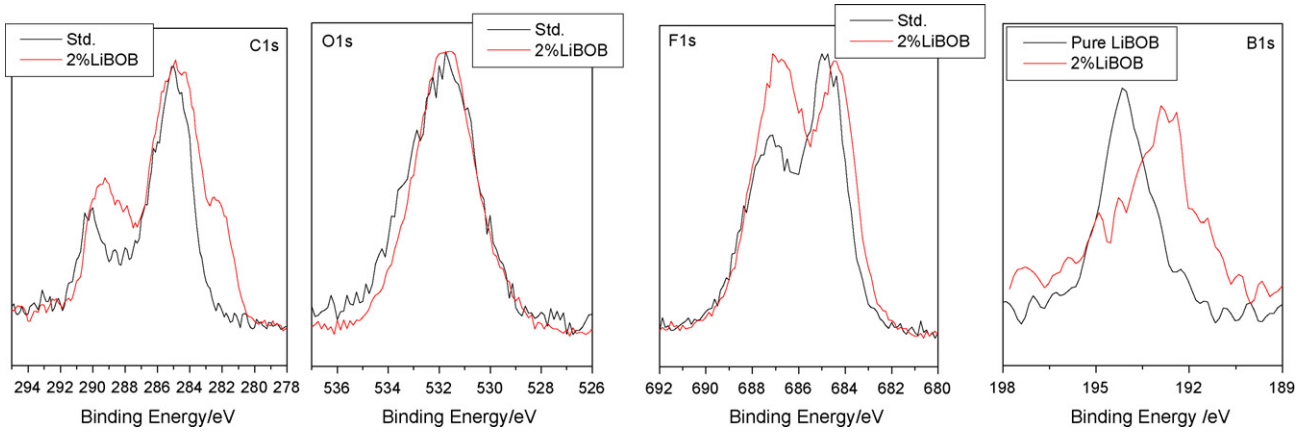

Fig. 7. C1s, O1s, F1s and B1s XPS spectra of std. vs. LiBOB sample on the anode.

Figs. 7–12 are normalized. Compared to standard sample, addition of DMAc or VC resulted in high concentrations of C and low concentrations of F, O and P. However, the LiBOB sample has a higher O concentration than standard anode, suggesting that the anode may be covered with $Li_xBF_yO_z$ and semi-carbonates from the decomposition reaction of LiBOB [14]. The high B concentration of samples containing LiBOB confirms that B is incorporated into the structure of SEI.

In contrast to the baseline anode, samples containing LiBOB–DMAc and VC–DMAc have a higher concentration of C, similar O, and lower F concentration. In addition, a higher concentration of C and O and but lower F is also found in the samples contain-

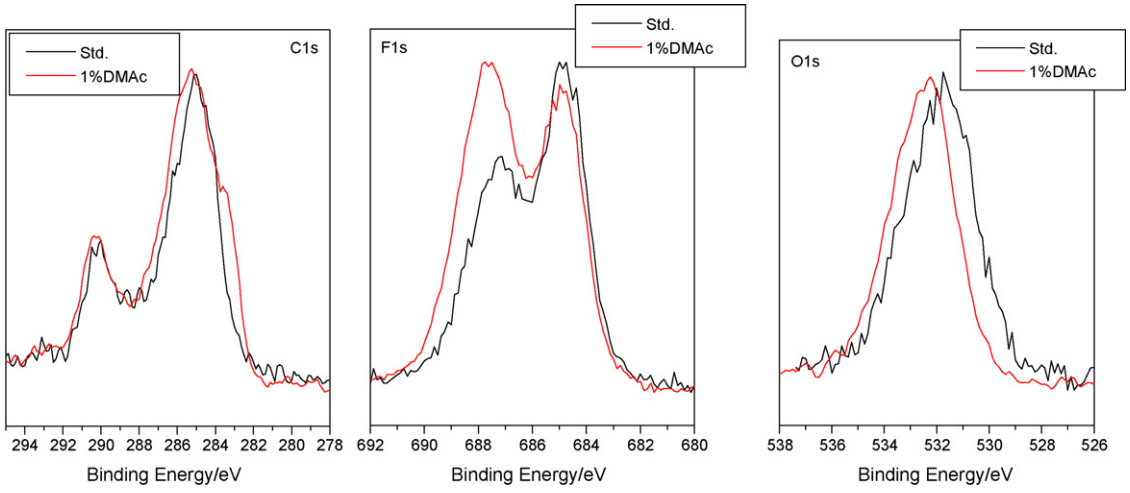

Fig. 8. C1s, O1s, and F1s XPS spectra of std. vs. DMAc sample on the anode.

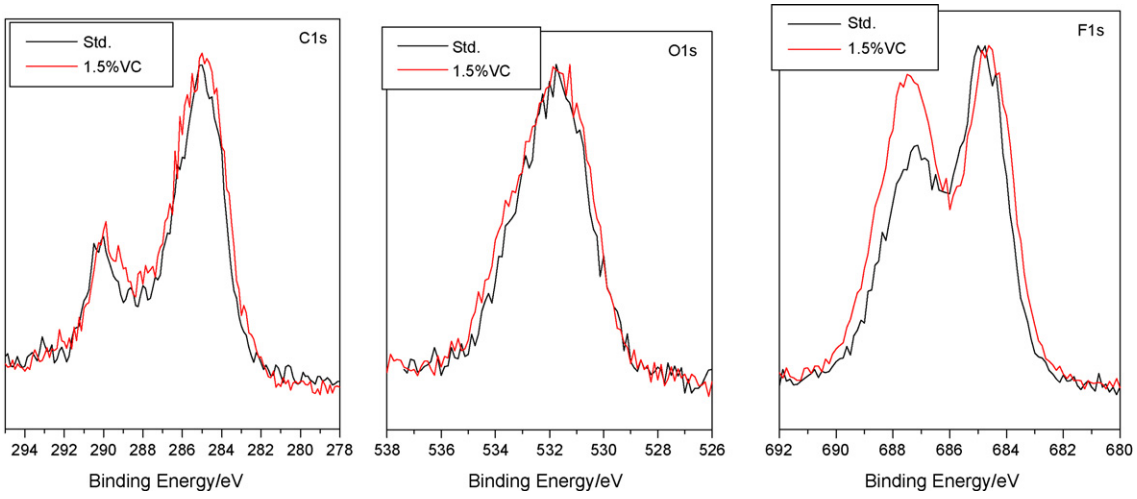

Fig. 9. C1s, O1s, and F1s XPS spectra of std. vs. VC sample on the anode.

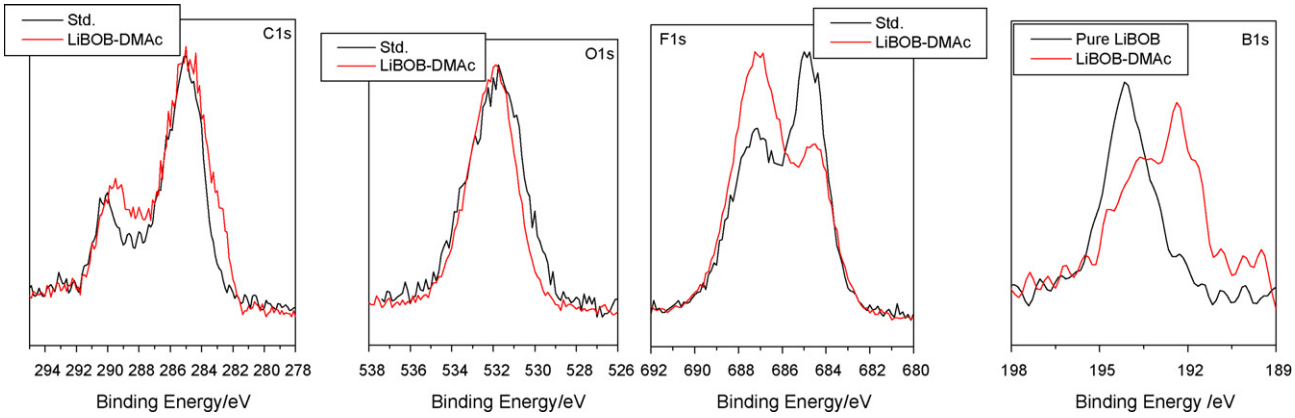

Fig. 10. C1s, O1s, F1s, and B1s XPS spectra of std. vs. LiBOB–DMAc sample on the anode.

ing LiBOB–VC and LiBOB–VC–DMAc compared to standard sample. Interestingly, the surface concentration of B for LiBOB–VC and LiBOB–VC–DMAc samples are lower than that from samples with only LiBOB as an additive. This may be due to a reaction between the reduction products of LiBOB and reduction products of VC.

The C1s, O1s, F1s and B1s XPS spectra of the anode extracted from a cell containing 2% LiBOB compared to the standard anode is depicted in Fig. 7. Both samples contain graphite at 284.3 eV in C1s spectra; hydrocarbons at 284.8 eV; C–O groups at 286 eV in C1s and 533 eV in O1s, lithium alkyl carbonates at 291.5 eV in C1s and 532.2 eV in O1s; Li_2CO_3 at 289.5 eV in C1s and 531.5 eV in O1s; PVDF at 290.5 eV in C1s and 687.7 eV in F1s; and LiF at 685 eV in F1s. However, compared to standard sample, the sample with 2% LiBOB has an abundance of semicarbonates characterized by the peak corresponding to 289 eV in C1s due to the ring-opening of the BOB^- anion and lithiated carbon at 282.5 eV in C1s. In addition, a relative reduction of LiF at 685 eV can be observed in F1s XPS spectrum, which verifies that LiBOB inhibits the formation of LiF on the SEI. In contrast to the pure LiBOB salt, the boron compound present on the anode in B1s spectrum is shifted from 194 eV to 192.5 eV,

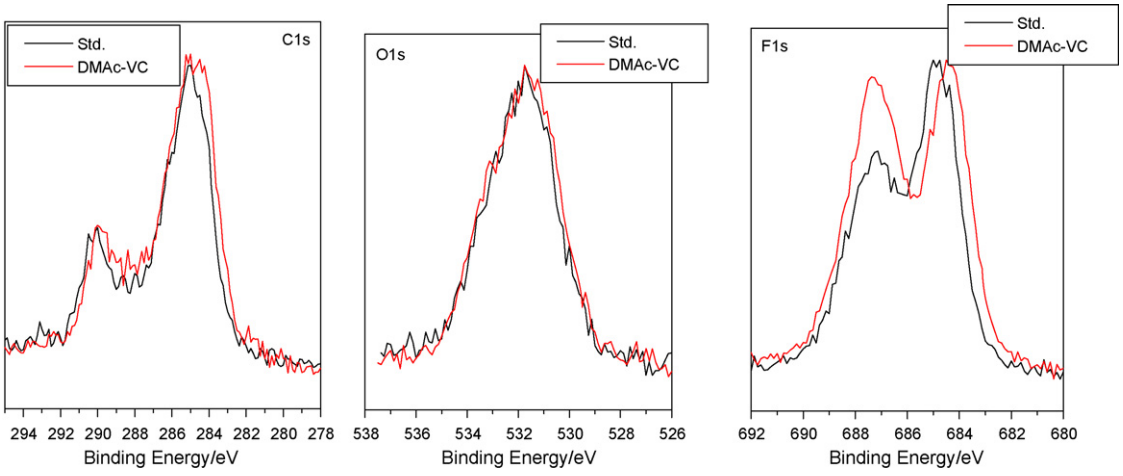

Fig. 11. C1s, O1s, and F1s XPS spectra of std. vs. VC–DMAc sample on the anode.

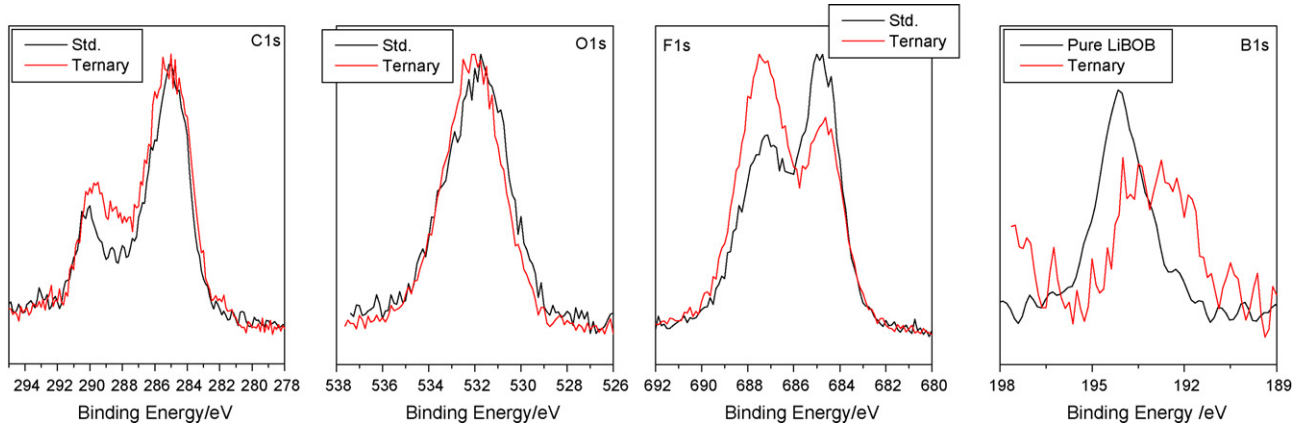

Fig. 12. C1s, O1s, F1s, and B1s XPS spectra of std. vs. ternary sample on the anode.

consistent with the ring-opening process of LiBOB and the generation of $Li_xBF_yO_z$ species [14,19].

Previous investigations indicate that DMAc binds the PF_5 generated during the thermal decomposition of $LiPF_6$ and stabilizes the electrolyte and the anode SEI [13]. Analysis of the surface of anodes extracted from cells containing DMAC, as shown in Fig. 8, suggest that the sample with DMAc has less LiF at 685 eV in F1 s than that of standard anode, suggesting that DMAc inhibits the decomposition of $LiPF_6$ and subsequent generation of LiF.

It has been reported that addition of VC inhibits the formation of LiF on the anode SEI after storage of cells at elevated temperature [13]. This is also confirmed for room temperature cycling, as shown in Fig. 9 with a relative decrease in the concentration of LiF at 685 eV in the F1s spectrum. Otherwise the surfaces of the anodes appear very similar.

Compared to the standard anode, the sample containing LiBOB–DMAc has more semicarbonates (289 eV, C1s) and lithiated carbon (282.5 eV, C1s) similar to the result of with LiBOB as additive in the electrolyte. The LiF is further reduced in the presence of LiBOB and DMAc. The concentration is significantly lower than samples with only LiBOB or DMAc (Fig. 10). This indicates that the combination of LiBOB and DMAc may be better than either of the single additives. As with the samples containing LiBOB, $Li_xBF_yO_z$ (192.5 eV, B1s) is observed upon addition of both LiBOB and DMAc in the electrolyte.

Upon Ar^+ ion sputtering, the boron is rapidly removed from the surface of the sample containing LiBOB and DMAc, suggesting a thin layer of borates. Alternatively, the boron was retained for a much longer sputtering time in samples containing only LiBOB as an additive, consistent with thicker layers of organoborates.

As shown in Fig. 13, the cathode extracted from the cell with added DMAc and VC has a higher concentration of graphite (284.3 eV, C1s) and lower concentration of LiF (685 eV, F1s) on the surface of the SEI than the standard sample.

A clear shoulder can be identified at 289 eV in C1s, characteristic of semicarbonates for the anode extracted from a cell containing LiBOB–VC. The increased intensity of C–O linkage (286 eV, C1s and 533 eV, O1s) indicates the formation of polymer or oligomer compounds on SEI. LiF (685 eV in F1s) was inhibited by LiBOB–VC combination. The peak at 192.5 eV in B1s is attributed to tricoordinated boron oligomers.

Upon initial Ar^+ ion sputtering, the concentration of C and B increase while O, F, and P decrease. This is quite different than what is observed for the sample with only LiBOB or the sample with LiBOB and DMAc. The reaction between LiBOB and VC appears to alter the structure of the anode SEI when compared to the SEI induced by either LiBOB or VC.

The structure of SEI generated in the presence of a ternary mixture of additives, LiBOB–VC–DMAc, is similar to that of LiBOB–VC binary mixture of additives. Semicarbonates (289 eV, C1s) and $Li_xBF_yO_z$ are easily distinguished (Fig. 12). LiF (685 eV, F1s) is reduced more than with any single additive, suggesting that the ternary combination may be beneficial to cells. The surface atomic concentration changes quickly upon sputtering to reveal a high concentration of C and very low concentrations of O, F, P and B consistent with a thinner anode SEI than observed for the other samples.

3.5. XPS of surface layer on the cathode

As mentioned above in the section discussing the IR-ATR results, the modifications to the cathode resulting from the incorporation of additives is much smaller than observed for the SEI on the anode. XPS spectra of cathodes provide similar results. As previously reported, the surface of $LiNi_{0.8}Co_{0.2}O_2$ is covered by a layer of Li_2CO_3. In contrast to the baseline cathode, all samples with

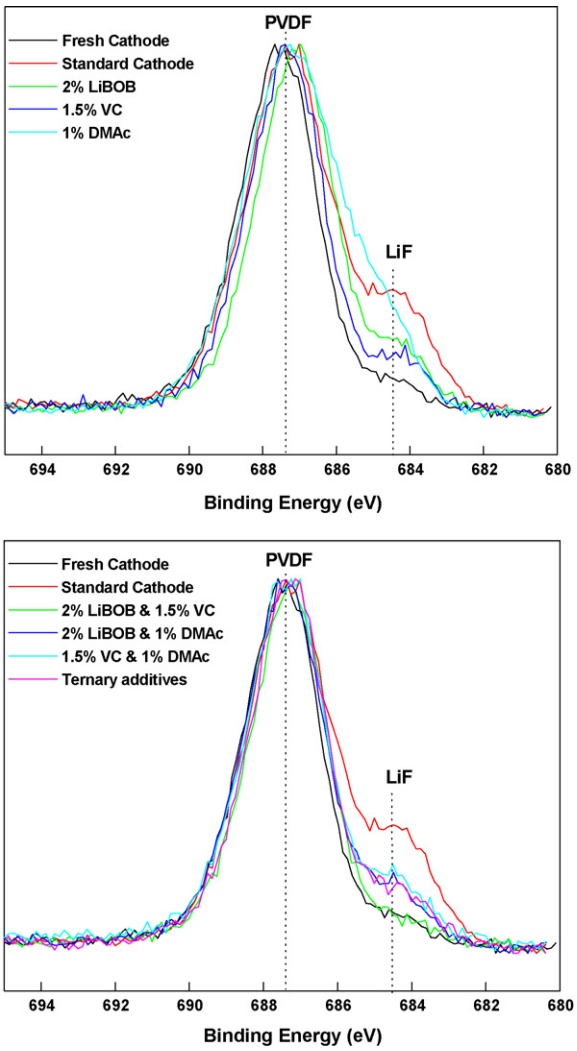

Fig. 13. F1s XPS spectra of cathode from cells with a single additive (top) and multiple additives (bottom).

additives have a stronger signal at 289 eV and 531.5 eV in C1s and O1s spectra, suggesting that more surface Li_2CO_3 is retained in the presence of additive in the electrolyte. Compared to the standard sample, the weaker signals at 529 eV in O1s, characteristic of the bulk metal oxide, further confirm that bulk metal oxides are less exposed to the electrolyte due to more retained Li_2CO_3. The most striking difference between additive samples and baseline cathode is observed in the F1s spectra (Fig. 13), which show that the cathodes extracted from cells containing additives have less resistive LiF (685 eV, F1s) on the surface of cathode.

4. Conclusion

A combination of thermal stabilizing additives with different mechanisms of stabilization has been investigated in LIBs containing $LiPF_6$/carbonate electrolytes. The combinations have a additive effect on cell performance suggesting that the different types of additives can work together to generate a greater benefit than is observed with a single additive. While we expect that the use of similar anode and cathode materials would yield similar results, we are currently conducting related investigations with different cathode materials to investigate the generality of the effects observed in this investigation. These results will be reported in due course.

Acknowledgements

We thank the US Army Research Laboratory (contract no. W911QX-07-C-0026 to Yardney Technical Products) and the Batteries for Advanced Transportation Technologies (BATT) Program supported by the U.S. Department of Energy Office of Vehicles Technologies for financial support of this research.

References

[1] D.P. Abraham (Ed.), Diagnostic examination of generation 2 lithium-ion cells and assessment of performance degradation mechanisms, Advanced Technology Development Program for Lithium-ion Batteries, U.S. Department of Energy, 2005.
[2] C. Campion, W. Li, W.B. Euler, B.L. Lucht, B. Ravdel, J. DiCarlo, R. Gitzendanner, K.M. Abraham, Electrochem. Solid State Lett. 7 (2004) A194–A197.
[3] C.L. Campion, W. Li, B.L. Lucht, J. Electrochem. Soc. 152 (2005) A2327–A2334.
[4] E. Peled, J. Electrochem Soc. 126 (1979) 2047.
[5] M. Broussely, Ph. Biensan, F. Bonhomme, Ph. Blanchard, S. Herreyre, K. Nechev, R.J. Staniewicz, J. Power Sources 146 (2005) 90.
[6] K. Tasaki, K. Kanda, T. Kobayashi, S. Nakamura, M. Ue, J. Electrochem. Soc. 153 (2006) A2192.
[7] K. Xu, U. Lee, S. Zhang, M. Wood, T.R. Jow, Electrochem. Solid State Lett. 6 (2003) A144.
[8] K. Xu, S. Zhang, T.R. Jow, Electrochem. Solid State Lett. 8 (2005) A365.
[9] A. Xiao, L. Yang, B.L. Lucht, Electrochem. Solid State Lett. 10 (2007) A241.
[10] A. Xiao, W. Li, B.L. Lucht, J. Power Sources 162 (2006) 1282.
[11] D. Aurbach, Y. Ein-Eli, O. Chusid, Y. Carmeli, M. Babai, H. Yamin, J. Electrochem. Soc. 141 (1994) 603.
[12] M. Herstedt, D.P. Abraham, J.B. Kerr, K. Edstrom, Electrochem. Acta 49 (2004) 5097.
[13] W. Li, A. Xiao, B.L. Lucht, M.C. Smart, B.V. Ratnakumar, J. Electrochem. Soc. 155 (2008) A648–A657.
[14] A. Xiao, L. Yang, B.L. Lucht, S.-H. Kang, D.P. Abraham, J. Electrochem. Soc. 156. (2009).
[15] G.V. Zhurang, P.N. Ross, Electrochem. Solid State Lett. 6 (2003) A136.
[16] K. Edstrom, M. Herstedt, D.P. Abraham, J. Power Sources 153 (2006) 380.
[17] H. Ota, Y. Sakata, A. Inoue, S. Yamaguchi, J. Electrochem. Soc. 151 (2004) A1659.
[18] D. Aurbach, K. Gamolsky, B. Markovsky, Y. Gofer, M. Schmidt, U. Heider, Eletrochem. Acta 47 (2002) 1423.
[19] K. Xu, U. Lee, S.S. Zhang, T.R. Jow, J. Electrochem. Soc. 151 (2004) A2106.